

Antitwilight II: Monte Carlo simulations

STEVEN C. RICHTSMEIER,^{1,*} DAVID K. LYNCH,² AND DAVID S. P. DEARBORN³

¹Spectral Sciences, Inc. 4 Fourth Avenue, Burlington, Massachusetts 01803-3304, USA

²Thule Scientific, P.O. Box 953, Topanga, California 90290, USA

³Lawrence Livermore National Laboratory, Livermore, California 94550, USA

*Corresponding author: s.richtsmeier@spectral.com

Received 27 February 2017; revised 6 April 2017; accepted 7 April 2017; posted 10 April 2017 (Doc. ID 287554); published 12 June 2017

For this paper, we employ the Monte Carlo scene (MCScene) radiative transfer code to elucidate the underlying physics giving rise to the structure and colors of the antitwilight, i.e., twilight opposite the Sun. MCScene calculations successfully reproduce colors and spatial features observed in videos and still photos of the antitwilight taken under clear, aerosol-free sky conditions. Through simulations, we examine the effects of solar elevation angle, Rayleigh scattering, molecular absorption, aerosol scattering, multiple scattering, and surface reflectance on the appearance of the antitwilight. We also compare MCScene calculations with predictions made by the MODTRAN radiative transfer code for a solar elevation angle of $+1^\circ$. © 2017 Optical Society of America

OCIS codes: (010.0010) Atmospheric and oceanic optics; (010.1300) Atmospheric propagation; (010.1320) Atmospheric transmittance; (010.1690) Color; (290.4210) Multiple scattering; (290.5870) Scattering, Rayleigh.

<https://doi.org/10.1364/AO.56.00G169>

1. INTRODUCTION

Twilight is sunlight scattered by the atmosphere that is visible when the Sun is below the horizon. In a companion paper [1] to the present work, Lynch *et al.* describe a series of visual observations of the antitwilight made with the Sun moving beneath the observer horizon under “very clear or cloud-free” conditions. They name four principal visual components of the antitwilight, including (1) the blue “upper sky,” which extends downward from observer zenith; (2) the reddish “Belt of Venus”; (3) the “blue band,” which lies below the Belt of Venus and is part of the Earth’s shadow; and (4) the “horizon band,” a band of sky lying between the blue band and the horizon, which, though it lies farther into Earth’s shadow, is slightly brighter than the blue band. The evolution of these features was observed as a function of solar elevation angle.

Researchers have been attempting to model the twilight sky for many decades. Lee [2] provides a good historical perspective. To adequately model the radiation transport requires treatment of several physical phenomena, including Rayleigh scattering, molecular absorption, aerosol scattering, multiple scattering, and refraction, all for a vertically varying 3D spherical atmosphere. The model must also support placement of the Sun below the observer’s horizon. Surface reflections may contribute to twilight sky brightness as well. Monte Carlo techniques would seem to be the most straightforward method to attack the problem, and the capabilities of modern computer hardware have considerably reduced the drawbacks of the extreme computational requirements of Monte Carlo methods.

In order to help us understand the colors and structure of the antitwilight, we have employed the MCScene code [3,4]. MCScene is a first-principles 3D radiation transport model, which predicts both solar and thermal spectral channel radiances using a direct simulation Monte Carlo technique. Atmospheric optical properties are defined via spectral databases generated by MODTRAN [5]. Photon trajectories are followed along reverse paths (from the observer), scattering off atmospheric particles and molecules, and reflecting off the topographic background as well as any inserted objects. Statistics on the observed radiance are accumulated at each interaction. MCScene supports 3D water and ice clouds and spatially structured surface channel reflectances. It addresses the wide range of criteria necessary to model the twilight sky, except for refraction. Also, note that, like MODTRAN, MCScene treats the Sun as a point source. We will demonstrate that, while the neglect of refraction results in the over-prediction of radiant intensities for low and sub-horizon solar angles, it does not adversely affect twilight sky spatial structure. The goal of our simulations is to reproduce the structure and colors of the antitwilight, including formation and evolution of the horizon band, the blue band, the Belt of Venus, and the upper sky, as the Sun moves further below the horizon. In addition to exploring the underlying physics giving rise to these features, we will also examine the effects of surface albedo and aerosol load on the brightness and colors of the antitwilight.

2. COMPARISON TO IMAGERY

There was no measurement of aerosol load to accompany the video and photo observations mentioned above [1], so, given

the “very clear and cloud-free” criterion for collection of the imagery, our initial simulations assume no aerosols present. We used MODTRAN’s “mid-latitude winter” atmosphere model for atmosphere species profiles. Also, because the observations took place over the ocean, we start by assuming uniform black terrain everywhere. The simulated sensor was situated on the ground at sea level. For comparisons with imagery, the sensor had three spectral channels with Gaussian-shaped response functions centered at 452, 561, and 596 nm for channels designated “blue,” “green,” and “red,” respectively. Their full widths at half-maximum are 51, 96, and 80 nm. Output from MCScene is in radiance units. However, given that the video and photo observations described above were not radiometric measurements, we do not make absolute radiant intensity comparisons between model results and observations. The brightness of modeled imagery is typically scaled to fill the dynamic range of 24 bit RGB color space.

Figure 1 shows our first comparison. The video frame is from a Pismo Beach, CA, observation of 31 December

2015, Sun at the observer’s back and 1° below the horizon. The FOV for the MCScene simulation measures $60^\circ \times 60^\circ$ with the observer elevation angles running from $+1^\circ$ at bottom to 61° at top. MCScene has reproduced the gross features of the observations: the dark shadow of the Earth (blue band) near the horizon, the brightening of the sky into the reddish Belt of Venus with increasing elevation angle, the whitening of the sky above the BV, and the bluing of the upper sky. MCScene’s rendering of the upper sky is perhaps too blue, while the coloring of the lower sky appears to be more accurate.

In Fig. 2, a still photo taken from Westward Beach in Malibu, CA, on 15 September 2015 with the Sun at the observer’s back 4° below the horizon is compared with another MCScene simulation for the same solar position. Again, the FOV for the MCScene simulation measures $60^\circ \times 60^\circ$ with the observer elevation angles running from $+1^\circ$ at bottom to 61° at top. The MCScene calculation replicates the antitwilight structures noted by Lynch *et al.* [1]. The relatively bright



Fig. 1. Video frame (left) and MCScene simulation (right) comparison for $\epsilon = -1^\circ$.

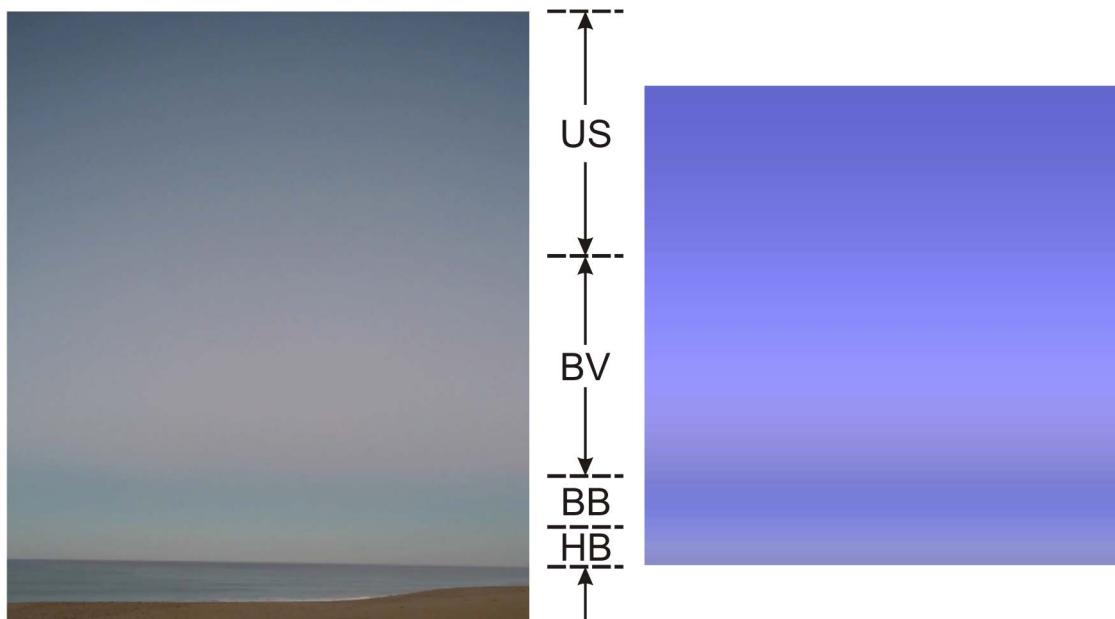


Fig. 2. Still photo (left) and MCScene simulation (right) comparison for $\epsilon = -4^\circ$. Indicated are the upper sky (US), the Belt of Venus (BV), the blue band (BV), and the horizon band (HB).

“horizon band” extends upward a few degrees from the horizon. Above the horizon is the darker “blue band” that is easily distinguished from the “Belt of Venus” above and the “horizon band” below. The sky brightens slightly above the blue band and has a slightly reddish cast—the Belt of Venus, which gradually fades into the blue “upper sky.” As is the case for Fig. 1, the MCSScene sky of Fig. 2 is too blue. That said, MCSScene produces the spatial structures of Figs. 1 and 2 purely with Rayleigh scattering.

3. RGB SIMULATION SEQUENCE

Figure 3 shows MCSScene simulations of the antitwilight sky for a series of solar elevations running from $+1^\circ$ to -4° . Superimposed on the imagery are the simulated radiance profiles as a function of observer elevation α for the blue, green, and red spectral channels defined above. For $\epsilon = +1^\circ$, the Sun is just above the horizon at the observer’s back. As the observation angle moves down from the top of the image, the radiance profile for each band increases to a maximum within several degrees of the horizon, after which the radiance decreases until the horizon is reached. For the red channel, the radiance maximum occurs at about 4° . For the blue channel, the maximum radiance occurs higher in the sky—at about 11° . The appearance of the sky is yellow near the horizon as the red and green channels have similar contributions. At $\alpha = 1^\circ$, radiance in the blue channel is at least a factor of 2 smaller than

the other channels. This, and the fact that the peak in the blue radiance profile occurs at a higher altitude, is due to the increase in extinction of the Sun’s rays by Rayleigh scattering as the rays must travel through a denser atmosphere at lower altitudes. The extinction cross section is significantly greater at shorter wavelengths. At about $\alpha = 8^\circ$, the sky whitens as the radiance from the blue, green, and red channels cross each other. Above this elevation, the sky becomes bluer as the radiance in the blue channel increases to its maximum at 11° , then dims but remains blue as elevation is increased. Where Rayleigh scattering at low elevations resulted in a bias against blue light, the same higher scattering cross section favors blue light at higher altitudes, resulting in, as we know, a predominantly blue sky.

As the solar elevation moves to 0° , then -1° , the radiance maxima for all bands move to progressively higher elevations. The yellow color apparent near the horizon for $\epsilon = +1^\circ$ takes on a progressively redder hue and stretches higher above the horizon until, for $\epsilon = -1^\circ$, the Earth’s shadow becomes apparent along the horizon at $\alpha = 1^\circ$. The dominant color at the horizon is now blue.

As ϵ moves to -2° through to -4° , the maxima in the radiance profiles move to higher elevations. The Earth’s shadow in the atmosphere becomes larger as the Sun descends farther, and the Belt of Venus rides above the shadow and becomes progressively dimmer. The radiance profiles no longer show single maxima. A local minimum develops in the radiance profiles at the top of Earth’s shadow, and, at $\epsilon = -4^\circ$, there is a distinct

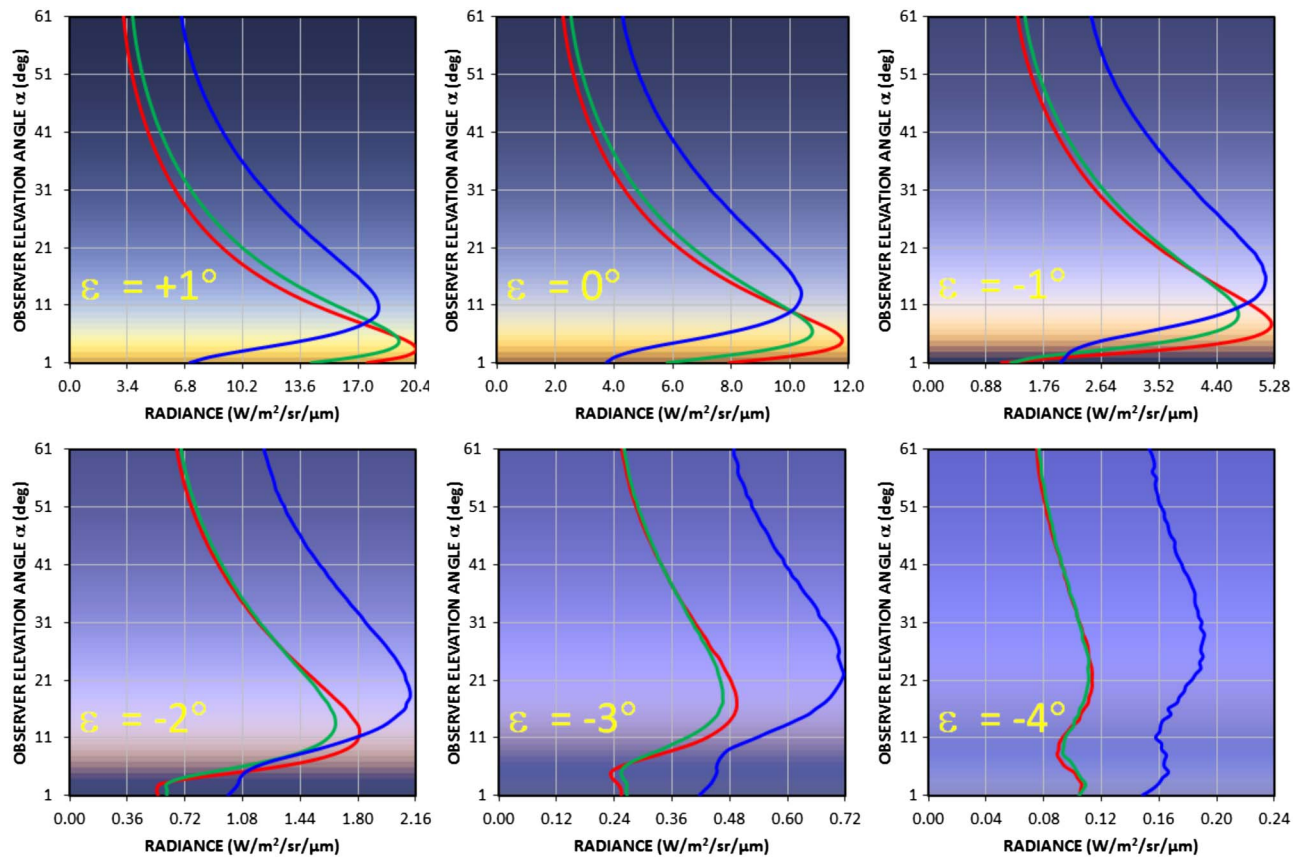


Fig. 3. MCSScene simulations of antitwilight for several solar elevations ϵ . Superimposed on the images are radiance profiles as a function of observer elevation α for the blue, green, and red spectral channels.

local maximum near the horizon in all bands. These local maxima are not appreciably more dim than the maxima that occur at $\alpha = 20\text{--}30^\circ$. The pure blue color of the “blue band” happens to occur where there is a local maximum in the blue channel radiance profile and local minima in the red and green channel profiles.

4. MULTIPLE SCATTERING CONTRIBUTIONS

The physics of the Earth shadow region visible in the antitwilight sky are more complex than just a simple shadow cast by the hard Earth through the atmosphere [6]. The shadow is not devoid of light to an observer as radiance from multiple scattering backfills the shadow, and this radiance is colored by the preference of Rayleigh scattering for shorter wavelengths, and by molecular absorption, predominantly by ozone, in the atmosphere. MCScene can help to elucidate the processes involved by accumulating statistics for scattering order contributions to computed radiance. Figure 4 shows MCScene scattering order contributions to the antitwilight radiance for each of the spectral channels as a function of observer elevation angle for solar angles of $+1^\circ$ (left), -1° (center), and -4° (right). Though photon trajectories with as many as 13 scattering

events were tallied, only scattering orders up to 4 were found to be statistically significant. In Fig. 4, with the Sun 1° above the horizon, the radiance at almost all elevations is dominated by single scattering. The exception to this is for the blue channel near the horizon. For all channels, the second order scattering contribution increases with decreasing α . For the blue channel, the second order contribution equals the first order contribution at $\alpha \approx 3^\circ$. In fact, at $\alpha = 1^\circ$, the third order contribution equals the single scattering contribution for the blue spectral channel.

When the Sun moves to $\epsilon = -1^\circ$, the Earth’s shadow becomes apparent in the single scattering curves in all spectral channels. In the shadow, second order scattering is the principal radiance contributor, though for the blue channel, third order and even fourth order scattering are statistically significant. For the red and green channel radiance profiles, the first order curves go to zero at $\alpha = 1^\circ$. The hard Earth is blocking illumination of the atmosphere at this elevation. Now, notice that the first order curve for the blue channel goes to zero at 3° . The shadow of the hard Earth does not vary spectrally. The extra 2° of shadow in the blue channel is due to the enhanced extinction of blue light by the dense lower atmosphere.

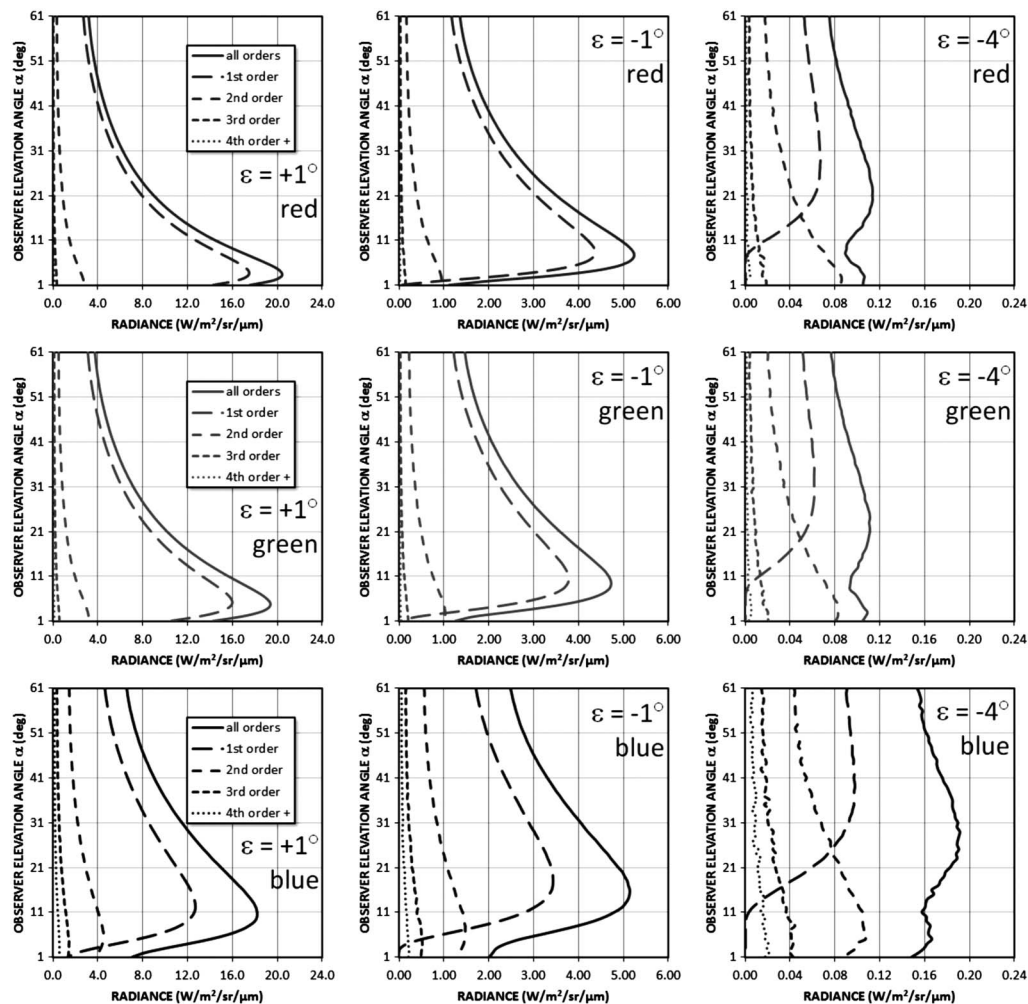


Fig. 4. MCScene calculations for scattering order contributions to the antitwilight radiance in the red (top row), green (middle row), and blue (bottom row) bands as a function of observer elevation angle for solar angles of $+1^\circ$ (left), -1° (center), and -4° (right).

For $\epsilon = -4^\circ$, the total radiance profiles for all three spectral channels have developed two local maxima separated by a local minimum. The Earth's shadow, i.e., the elevation where the single scattering contribution to the total radiance goes to zero, is at $\sim 8^\circ$ for the red and green channels and at 10° for the blue channel. The maxima at higher elevation α have about 50% contribution from single scattering, with the remaining contributions from higher order scattering. Local minima occur at α where the rapidly decreasing first order radiance goes to zero. Local maxima at lower elevation α occur at the maxima in the second order radiance profiles for each band. Generally speaking, most of the radiance to be observed in the horizon band and blue band is due to second order scattering, though for the blue spectral channel and $\epsilon = -4^\circ$, we see contributions for scattering order $N > 2$ of up to 35% of the total radiance.

5. SPECTRAL PREDICTIONS

The variation of color in the antitwilight sky, especially for the zero aerosols cases we have presented so far, is governed by just a few factors. (a) For an observer to see radiance from the antitwilight sky, sunlight must travel through the atmosphere and beyond the observer then be scattered back into the observer's line-of-sight. The base color is the top-of-the-atmosphere solar irradiance curve, approximately a blackbody of 5780 K. (b) With the Sun below the horizon, some photons are blocked by the Earth's hard surface, and the Earth's shadow is cast into the lower sky of the observer. (c) When sunlight must travel through the dense lower atmosphere, this discriminates against transmission of shorter wavelengths due to the $1/\lambda^4$ dependence of the Rayleigh scattering cross-section, a band of the antitwilight sky is illuminated with predominantly red light, and this light is scattered back into the observer's LOS for elevations just above the Earth's cast shadow. This is the Belt of Venus. (d) When the Sun's rays travel higher through the atmosphere, we have an optically thin scenario in which single scattering is the dominant pathway. Photons travel from the Sun, past the observer unattenuated, and are scattered back into the observer's LOS by a single scattering event. This favors shorter wavelength light, again due to the $1/\lambda^4$ dependence of the Rayleigh scattering cross-section. The sky is blue. (e) For the observer looking into the region of the Earth's shadow, radiance observed is due to multiple scattering. Photons that have already undergone at least one scatter, predominantly from the upper sky, are scattered down to the observer LOS where they are scattered back toward the observer. These photons are mostly blue, for the same reason the upper sky is blue. The path from the location of the first scatter to the scatter in the observer LOS is mostly vertical, and so this path has low optical depth. Therefore, the highest probability for the second scatter occurs near the ground, where the atmosphere is most dense. This gives rise to the horizon band.

Molecular absorption will influence sky radiance as well. Ozone, oxygen, and water will all absorb appreciable solar radiation in the visible spectral regime. Figure 5 shows a MODTRAN calculation of anti-solar sky radiance for a solar elevation angle of $+1^\circ$ and observer elevation angle of 3° . The atmosphere used was MODTRAN's mid-latitude winter model, no aerosols, and surface reflectance was uniformly

black. The top (dashed) curve in Fig. 5 shows the expected spectral radiance in the absence of molecular absorption. The lower (solid) curve shows the predicted radiance when molecular absorption is included in the calculation. The hashed areas indicate radiance absorbed by molecular species. Oxygen is uniformly mixed in the atmosphere, and so its effect on spectral radiance should be fairly consistent for a given measurement scenario. There is a seasonal dependence to MODTRAN's ozone profiles, with roughly 10% more O_3 column amount in winter than in summer. Water column amount also can vary widely. For example, the calculation of Fig. 5 assumed MODTRAN's mid-latitude winter model, a relatively dry atmosphere. On the other hand, the water column amount for the mid-latitude summer model is 3.4 times larger than for the mid-latitude winter model. Increased water column would affect predominately the longer wavelengths of the visible spectral regime, resulting in fewer "red" photons contributing to the spectral signature.

Figures 6–8 present visible spectra calculated by MCScene for various points in the antitwilight sky for three solar elevations. Figure 6 is the $\epsilon = -4^\circ$ case. Plotted are spectra for $\alpha = 6^\circ$, the elevation of the blue band, $\alpha = 21^\circ$, the elevation of the maximum in the red channel radiance profile, and $\alpha = 28^\circ$, the elevation of the maximum in the blue channel profile. The three spectra are quite similar, characterized by two broad peaks centered at ~ 470 and 650 nm, separated by a broad local minimum centered at ~ 570 nm. The local minimum is due to ozone absorption. The curve for $\alpha = 6^\circ$ clearly shows a preference for shorter wavelengths. The difference between the $\alpha = 21^\circ$ and $\alpha = 28^\circ$ is quite subtle, with the radiance at shorter wavelengths being slightly more intense for $\alpha = 28^\circ$, and the longer wavelength radiance being slightly more intense for $\alpha = 21^\circ$.

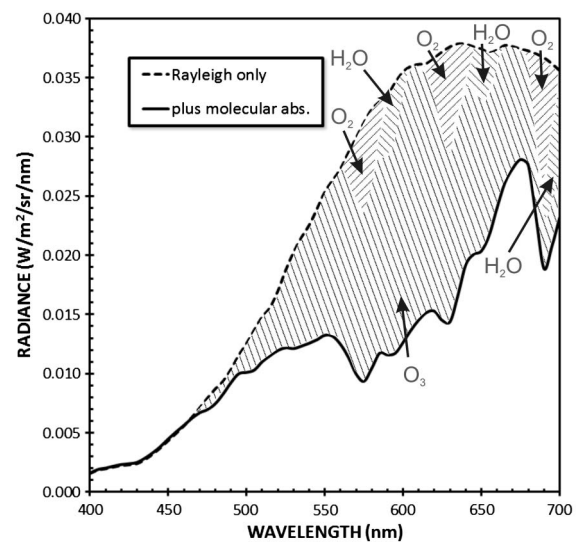


Fig. 5. MODTRAN predictions of antitwilight radiance for $\epsilon = +1^\circ$ and $\alpha = 1^\circ$. The dashed curve neglects the effects of molecular absorption, while the solid curve includes molecular absorption. The hashed areas indicate radiance absorbed by oxygen, water, and ozone. Spectral resolution is 10 nm.

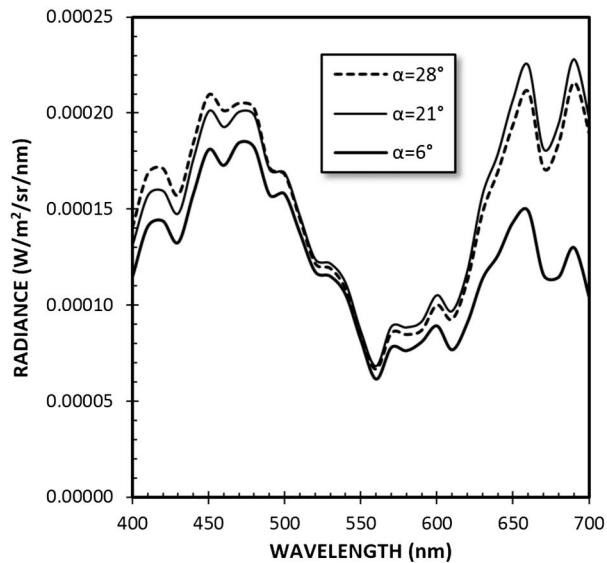


Fig. 6. Antitwilight spectra for three observer elevation angles for $\epsilon = -4^\circ$. Spectral resolution is 10 nm.

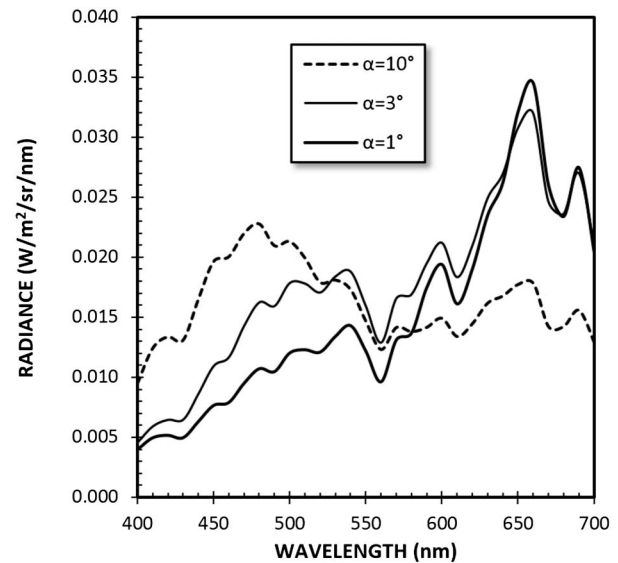


Fig. 8. Antitwilight spectra for three observer elevation angles for $\epsilon = +1^\circ$. Spectral resolution is 10 nm.

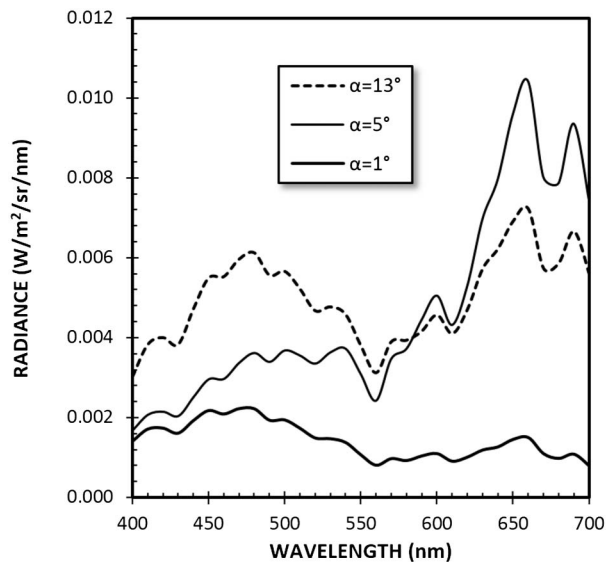


Fig. 7. Antitwilight spectra for three observer elevation angles for $\epsilon = -1^\circ$. Spectral resolution is 10 nm.

Figure 7 shows sample spectra for a case with the Sun 1° below the horizon. The curves shown in the figure include a spectrum from Earth's shadow ($\alpha = 1^\circ$), a spectrum from $\alpha = 5^\circ$ where the red spectral channel of the three-color simulations had a local maximum, and a spectrum from $\alpha = 13^\circ$ where the blue spectral channel exhibits a local maximum. The shadow spectrum is clearly the darkest of the three. This spectrum is most intense at shorter wavelengths, giving the dark segment its blue hue. For $\alpha = 5^\circ$, the radiance from shorter wavelengths is strongly diminished compared with longer wavelengths, and the sky here appears red. Here, blue light is scattered by the dense lower atmosphere before it can illuminate the antitwilight sky. Finally, at $\alpha = 13^\circ$, radiance from

shorter wavelengths has recovered from the extinction occurring at lower elevations, and we are in the single collision regime favoring shorter wavelengths yielding blue sky.

Finally, in Fig. 8, we show sample spectra for the case with the Sun 1° above the horizon. The elevation angles represented are $\alpha = 1^\circ, 3^\circ,$ and 10° . For $\alpha = 1^\circ$, the dark segment has been observed [1] near the horizon, even though the Sun is above the horizon, and no Earth shadow should be visible. The $\alpha = 1^\circ$ radiance curve is clearly darker than the two spectra above it at shorter wavelengths due to an "extinction shadow" cast by the dense lower atmosphere. This extinction shadow preferentially affects shorter wavelengths. This shadow is still evident at $\alpha = 3^\circ$, where blue wavelengths are still diminished in Fig. 8, and the sky appears yellow (red + green) in Fig. 3. At $\alpha = 10^\circ$, the Sun's rays are once again following an optically thin path, and Rayleigh scattering produces a blue sky. The dark segment observed at $\alpha = 1^\circ$ is dark only in a relative sense, as it is significantly "darker" than the sky above. In an absolute sense, the spectral radiance at 450 nm is actually more than three times as bright as the radiance for the hard Earth shadow for that wavelength and elevation with the Sun 1° below the horizon.

6. AEROSOL EFFECTS

The calculations presented to this point were all made assuming zero aerosol load. As we and others have noted, less hazy skies produce more vivid antitwilight colors. The effects of aerosols on the antitwilight sky are examined in Fig. 9. MCScene treats aerosol particles as Mie scatterers and uses scattering properties and profiles from MODTRAN [5]. We used MODTRAN's "rural" aerosol type and performed simulations for three aerosol vertical optical densities: $\tau_{\text{AER}} = 0, 0.032,$ and 0.064 . These are modest aerosol concentrations corresponding to 0, 10, and 20%, respectively, of the MODTRAN default column amount for this aerosol type. In Fig. 9, increasing the aerosol

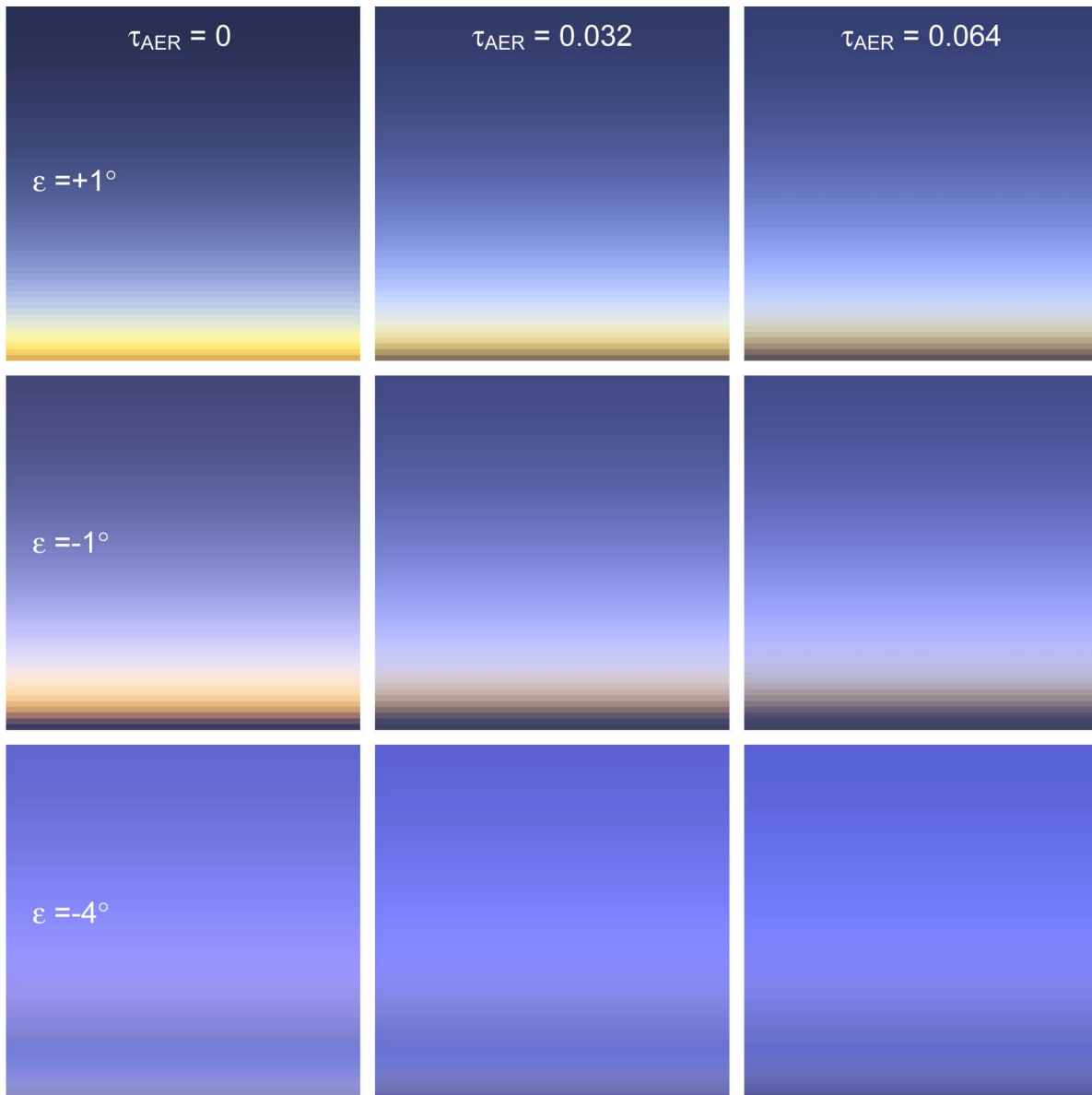


Fig. 9. Effect of increasing aerosol load ($l-r$) on antitwilight radiance for three solar elevations ϵ . Each image is scaled for maximum brightness.

amount for $\epsilon = +1^\circ$ and $\epsilon = -1^\circ$ noticeably diminishes the bright colors near the anti-solar horizon, and the sky at the horizon is darker. The aerosol density is greatest near the surface, and the diminished radiance with increasing aerosol load will be most noticeable when the Sun's rays have to travel long paths through the lower atmosphere. Single scatter albedos for the rural aerosol model are generally wavelength independent and have a value near 1. The extinction coefficient varies by about a factor of 2 over the 400–700 nm spectral range, so the wavelength dependence is not as strong as that of Rayleigh scattering.

With the Sun at $\epsilon = -4^\circ$, the color differences are not as striking. It does appear that the horizon band, evident within a few degrees of the horizon when there are no aerosols, is suppressed with increasing aerosol load. The horizon band arises from scattering of diffuse radiation from the denser atmosphere

near the ground. We do not fully understand the mechanism by which aerosols would suppress the horizon band, but perhaps light being scattered into the observer LOS at these elevation angles is attenuated by the intervening optical density of the aerosols.

7. EFFECT OF SURFACE ALBEDO

To this point, all of our calculations have assumed uniform black terrain. In MCScene, use of black terrain means that the trajectory of any Monte Carlo photon that strikes the ground is terminated. By assigning a positive surface albedo, light reflected from the ground may then contribute to sky radiance. Figure 10 shows MCScene simulations of the antitwilight sky for three solar elevations, as the surface albedo is increased from 0 to 0.5 to 1. Lambertian surface scattering

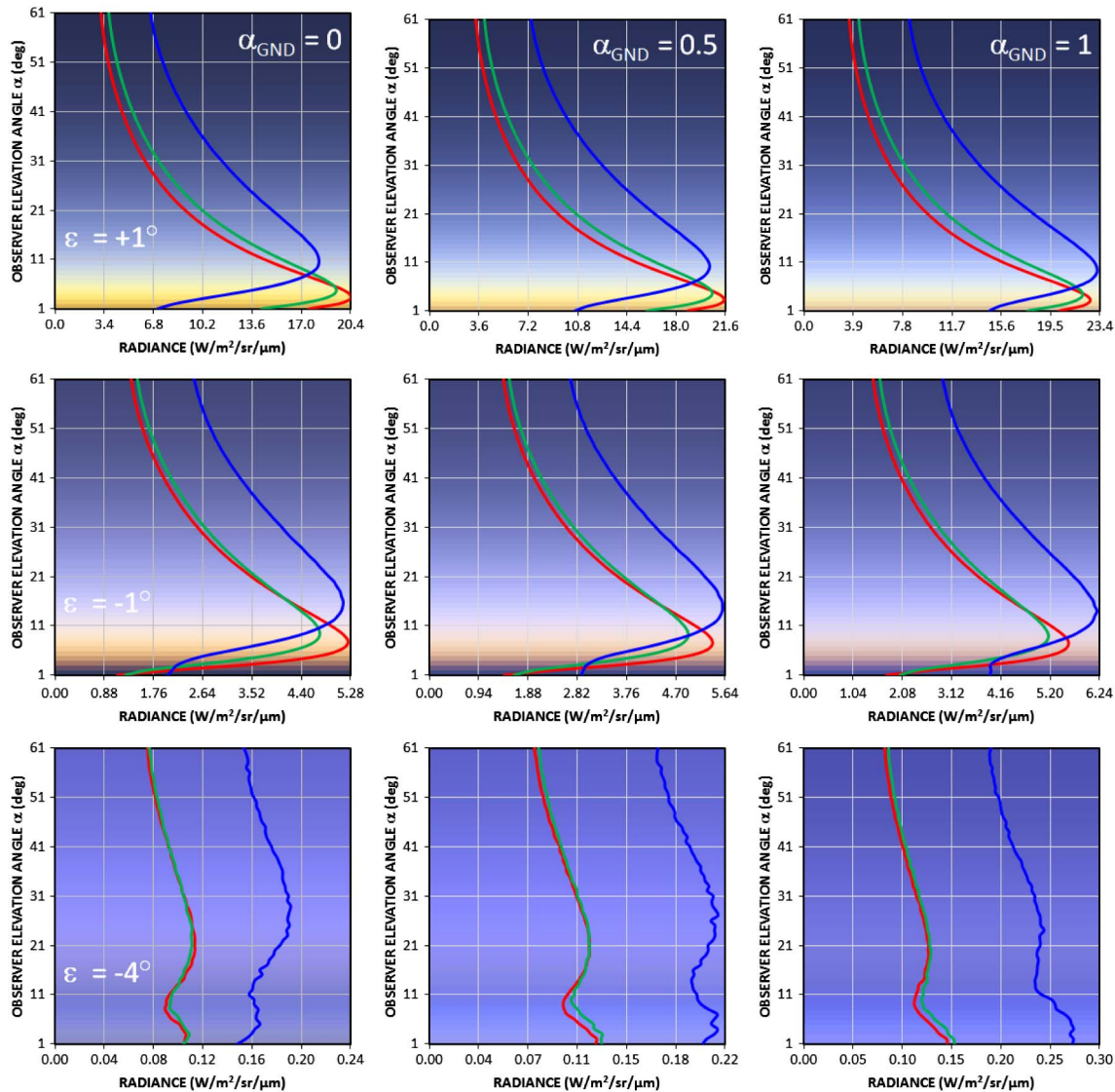


Fig. 10. Effect of increasing surface albedo α_{GND} (l-r) on antitwilight radiance for three solar elevations ϵ . Images are scaled to maximize use of RGB dynamic range.

is assumed, and once again, aerosols are removed from the simulations. Superimposed on the imagery are computed radiance profiles as a function of observer elevation angle α for the blue, green, and red spectral channels defined above. The images are scaled to maximize brightness.

There is very little apparent change in sky color with increasing surface albedo. The only subtle change in coloring is that the sky near the horizon for $\epsilon = -1^\circ$ appears to be more blue, as the surface albedo goes to 1. Examination of the radiance profiles for all cases shows that the relative contribution of the blue spectral band increases near the horizon for all three solar angles as surface albedo increases. This is due to increased contributions from higher order scattering. Figure 11 examines this in more detail.

In Figure 11, we plot scattering order contributions to the radiance profiles of the blue spectral band for $\epsilon = -4^\circ$ for surface albedos $\alpha_{\text{GND}} = 0$ (left) and 1 (right). With the Sun below the horizon, surface scattering cannot contribute to the first or

second order radiance profiles, and in fact, these curves are identical for $\alpha_{\text{GND}} = 0$ and $\alpha_{\text{GND}} = 1$. All enhancements to the radiance with increasing surface reflectance have to come from scattering order $N \geq 3$. The effect on sky color is complex, but the two extremes are having the surface reflection as the first scattering event or the second to last. (The last scattering event must be molecular scattering into the observer LOS.) If it is the first, it means the photon has struck the ground below the observer's horizon and scattered up into the sky toward the observer. The result is increased illumination of the observer's sky. There is no color selection associated with this event, as the surface here is uniformly white, and the net result would be an increase in radiance at all wavelengths. Examination of the radiance profiles of Fig. 10 at high elevations (single collision regime) shows increase in the radiance of all three spectral bands. Now, if the second to last scatter is the surface scatter, that means the photon has undergone previous Rayleigh scattering events, and so blue light is favored. These photons are

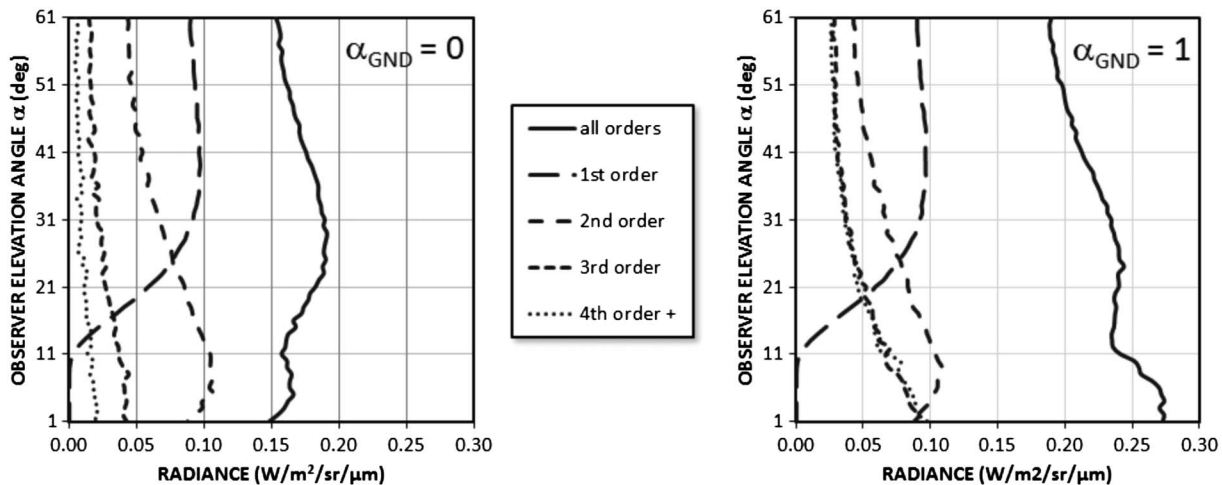


Fig. 11. Blue band scattering order contributions for $\epsilon = -4^\circ$ for surface albedos α_{GND} of 0 (left) and 1 (right).

more likely to scatter into the observer LOS near the ground where the atmosphere is denser. Enhancement to the blue spectral channel near the ground with increasing surface albedo was noted in Fig. 10. It is most noticeable in Fig. 11 where, with the Sun at $\epsilon = -4^\circ$, there is no first order scattering to obscure the higher order enhancement.

8. COMPARISON OF MCSCE WITH MODTRAN

The calculations above were performed with MCSce [3,4], which does not include refraction, but does allow the Sun to be below the horizon. MODTRAN [5], on the other hand, does calculate refraction, but only when the Sun is above the horizon. To link the two codes and further validate MCSce's results, we compared the results of each code with the Sun at an altitude ϵ of $+1^\circ$, a case where significant refraction occurs. Such a comparison allows us to estimate the error inherent in the MCSce simulations. For both codes, we utilized MODTRAN's mid-latitude winter atmosphere model, zero aerosols, and assumed uniform black terrain. Calculations were performed for three spectral channels with Gaussian-shaped response functions centered at 452, 561, and 596 nm for channels designated "blue," "green," and "red," respectively. Their full widths at half-maximum are 51, 96, and 80 nm.

Figure 12 shows the resulting radiance profiles for the anti-twilight sky. MCSce overestimates the radiance in all three bands for all elevations. For the red and green bands, MCSce radiances are 25%–40% greater than the corresponding MODTRAN radiances. For the blue band, the difference is 45%–60%, except at low observer elevation angles where the difference increases to a factor of 2. MCSce neglects refraction, while MODTRAN correctly calculates the refracted solar position. While MCSce and MODTRAN place the Sun at the same apparent position in the sky, when the Sun is low in the sky, the fact that MODTRAN's solar rays follow a refracted path means that they will encounter more atmosphere than MCSce's solar rays and thus be significantly more attenuated by the atmosphere. The effect will be greater at shorter wavelengths. The net result is that the absolute radiance

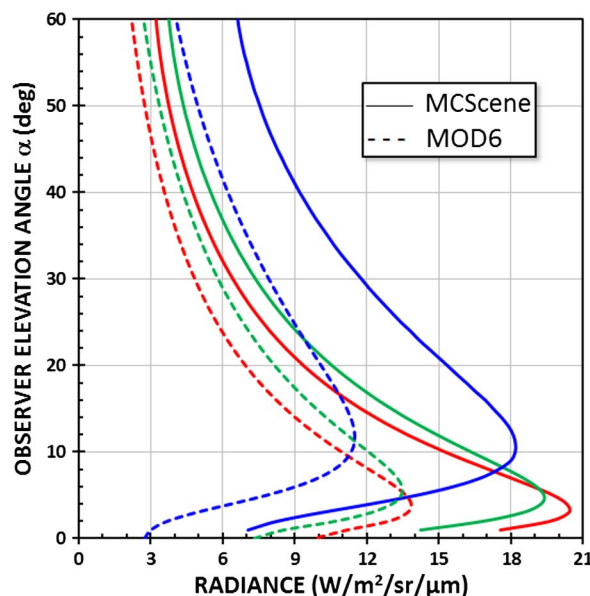


Fig. 12. MCSce (solid curves) versus MODTRAN6 (dashed curves) comparisons of anti-twilight radiance predictions for three spectral bands for $\epsilon = +1^\circ$.

estimates from MCSce presented above are slightly high, and the simulated images are a little too blue, due to neglect of refraction.

The MCSce versus MODTRAN comparison for this case is improved if we move the Sun in the MCSce calculation to $\epsilon = +0.5^\circ$, the geometric location of the Sun when the refracted position is $\epsilon = +1^\circ$. This does not give MCSce the capability to calculate a curved refractive path for incoming sunlight, but it does sample lower into the atmosphere as the true refractive path would. The result (see Fig. 13) shows that the discrepancy between the MCSce and MODTRAN calculations is reduced by at least a factor of 2 for all bands and observer elevations. We would expect that addition of support for refraction to MCSce would remove any further discrepancies.

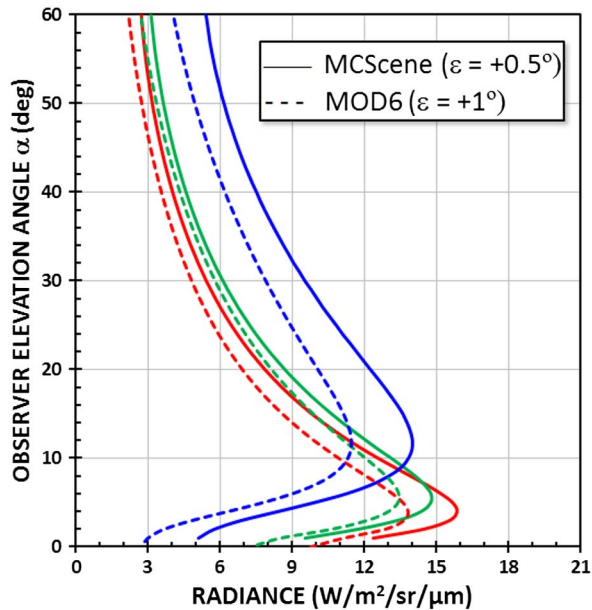


Fig. 13. Comparison of antitwilight radiance calculations from MCScene with a solar elevation angle $\epsilon = +0.5^\circ$ (solid curves) with MODTRAN6 calculations for $\epsilon = +1^\circ$ (dashed curves) for the three spectral bands of Fig. 12.

9. SUMMARY AND CONCLUSIONS

We have investigated the antisolar twilight sky using a first-principles 3D radiation transport model utilizing Monte Carlo techniques. The MCScene model reproduces many of the salient features of clear sky observations, including colors and spatial structures and their dependence on solar elevation angle. The role of multiple scattering was examined and was shown to explain the dependence of sky radiance on observer

elevation angle. The spectral dependence of sky radiance was investigated for various solar elevations and observer angles, and the effect of absorption by several molecular species was noted. Modest aerosol loads were found to diminish the bright sky colors on the anti-solar horizon, and surface reflectance was found to have only a small effect on antitwilight sky radiances. Finally, we compared a MCScene calculation for low Sun angle with a calculation from the MODTRAN radiative transfer code in order to assess how MCScene's neglect of atmospheric refraction might affect our results. We conclude that absolute radiances from MCScene are slightly overestimated, but that our conclusions concerning color, spatial structure, aerosol dependence, and surface reflectance dependence should be unaffected.

Acknowledgment. The authors would like to thank Raymond Lee, Jr. for many useful conversations about twilight. S. C. R. acknowledges support from the Internal Research and Development program of Spectral Sciences, Inc.

REFERENCES

1. D. K. Lynch, D. S. P. Dearborn, and S. C. Richtsmeier, "Antitwilight I: structure and optics," *Appl. Opt.* **56**, G156–G168 (2017).
2. R. L. Lee, Jr., "Measuring and modelling twilight's Belt of Venus," *Appl. Opt.* **54**, B194–B203 (2015).
3. S. C. Richtsmeier, A. Berk, S. M. Adler-Golden, and L. S. Bernstein, "A 3D radiative-transfer hyperspectral image simulator for algorithm validation," in *Proceedings of ISSSR*, Quebec City, Canada, June 2001.
4. F. T. Hawes, A. Berk, and S. C. Richtsmeier, "Development and validation of P-MODTRAN7 and P-MCScene, 1D and 3D polarimetric radiative transfer models," *Proc. SPIE* **9853**, 98530S (2016).
5. A. Berk, P. Conforti, R. Kennett, T. Perkins, F. Hawes, and J. van den Bosch, "MODTRAN6: a major upgrade of the MODTRAN radiative transfer code," *Proc. SPIE* **9088**, 90880H (2014).
6. J. Dubois, "Contribution a l'étude de l'ombre de la terre," *Annales de Géophysique* **7**, 103–135 (1951).